Polskie Towarzystwo Materiałów Kompozytowych
Polish Society of Composite Materials

25: 3 (2025) 166–180

COMPOSITES THEORY AND PRACTICE

ISSN (online): 2299-128X

Aleksandra Bąk [a]* (0009-0004-5879-8008), Bartosz Surówka [a], Ryszard Prorok [a] (0000-0002-1120-0732), Dominika Madej [a] (0000-0002-5418-1973)

[a] *AGH University of Krakow, Faculty of Materials Science and Ceramics, Department of Ceramics and Refractories, al. A. Mickiewicza 30 30-059 Krakow, Poland*
* *Correspondence:* aleksandraba@agh.edu.pl

Received (Otrzymano) 01.05.2025
Published on-line (Opublikowano) 30.09.2025

DEVELOPMENT OF THE PROPERTIES OF MAGNESIA ALUMINA SPINEL-BASED REFRACTORY COMPOSITES WITH MODIFYING OXIDES

https://doi.org/10.62753/ctp.2025.01.3.3

The present study investigates the synthesis of $MgAl_2O_4$ spinel via one-step sintering, producing a reference sample without additives and four additional samples containing 5 wt% ZrO_2, Fe_2O_3, SiO_2, or TiO_2, respectively. The MA sample along with the four types of modified spinel-based composites [MA_5T, MA_5Z, MA_5F, MA_5S] were characterized in terms of their phase composition, microstructure, bulk and true densities, as well as open and true porosities of the sintered materials. High-temperature microscopy was employed to evaluate dimensional changes of the samples during their heat treatment process. The presence of phases and the firing behavior of the resulting composite materials were evaluated using thermodynamic simulation (FactSage 8.3). The study demonstrated that the incorporation of specific oxide additives significantly influences the synthesis and properties of $MgAl_2O_4$ spinel. Iron (Fe^{3+}) and titanium (Ti^{4+}) ions were found to induce structural modifications within the spinel lattice, suggesting partial substitution or incorporation into the crystal framework. XRD analysis showed that the addition of the SiO_2 modifier leads to the formation of Mg_2SiO_4, which can partially dissolve into the spinel phase, while ZrO_2 promoted the extraction of Al^{3+} ions from the spinel structure, as corroborated by the thermochemical simulations using FactSage. The highest microstructural densification was achieved in the samples with TiO_2 and SiO_2, indicating their positive role in enhancing sintering efficiency. Conversely, the addition of Fe_2O_3 did not significantly affect the densification behavior, despite the formation of an Fe-rich spinel phase.

Keywords: spinel-based high-temperature ceramics, refractories, sintering, additives, composites

INTRODUCTION

Magnesia-alumina spinel ($Mg_{1+x}Al_{2-x}O_4$) has attracted significant attention in the refractory industry due to its exceptional properties, including a high melting point (2135°C), superior hardness, high chemical resistance, and a low thermal expansion coefficient [1–4]. Thanks to these outstanding features, magnesia alumina spinel is widely used in the cement industry in refractory lining, particularly in the burning and transition zones of rotary kilns, where it is employed to modify MgO-based refractory bricks and enhance their thermal and mechanical performance [5]. It also plays a crucial role in the steel industry, where it is utilized as a lining in steel ladles, well blocks, and porous plugs, offering good resistance to slag corrosion and excellent mechanical performance

at high temperatures [5, 6]. Additionally, magnesia alumina spinel is a component in the production of lightweight refractory aggregates with enhanced insulating properties, contributing to reduced overall lining weight without compromising compressive strength or thermal resistance [7]. Magnesia-alumina spinel is typically synthesized by a solid-state reaction between MgO and Al_2O_3 powders. The formation mechanism involves the interdiffusion of Mg^{2+} and Al^{3+} ions through a stable oxygen lattice, where Al^{3+} ions migrate from Al_2O_3 to MgO particles, and Mg^{2+} ions diffuse in the opposite direction, resulting in the formation of the $MgAl_2O_4$ spinel phase [2, 4–6, 8]. However, this reaction is accompanied by significant volume expansion of up to 8% [8, 9], which can lead to increased porosity. Consequently, extensive research has been devoted to exploring the effect of various sintering aids aimed at minimizing volume expansion and achieving a dense spinel structure. Numerous studies have investigated the influence of additives such as: LiF, $MgCl_2$, $AlCl_3$ [10], Y_2O_3, Eu_2O_3 [11], B_2O_3 [12], TiO_2 [13, 14], ZnO [15, 16], La_2O_3 [3], and ZrO_2 [17, 18] on MA sintering and its overall properties. Mohan et al. [10] investigated the effect of LiF, $MgCl_2$, and $AlCl_3$ on the formation and densification of magnesia alumina spinel. These additives have been reported to significantly enhance the spinel formation reaction, lower the sintering temperatures by promoting liquid phase formation and improve bulk density. Khomidov et al. [11] studied the influence of Y_2O_3 and Eu_2O_3 on $MgAl_2O_4$ prepared by sol-gel synthesis. They found that rare earth oxides effectively facilitated sintering. An addition of 1.5 wt% Eu_2O_3 reduced the peak spinel formation temperature to 900°C at a firing time of 240 min, while 3 wt% Y_2O_3 was needed to maximize the spinel formation at this temperature. B_2O_3 was also considered by Lemeshev et al. [12] as an additive to promote the synthesis of transparent spinel ceramics. The results showed that the B_2O_3 addition helps to form denser samples with a lower porosity. Naghizadeh et al. [14] investigated the effect of the addition of TiO_2 on the phase evolution and microstructure of $MgAl_2O_4$ spinel. The study found that the TiO_2 addition refines the grain size and strengthens the microstructure of $MgAl_2O_4$ ceramics. This led to a denser microstructure with fewer pores and a more uniform grain size distribution, which was due to liquid phase sintering and the formation of new phases at the grain boundaries. Ghosh et al. [15] studied the effect of an ZnO addition on the densification and properties of magnesia alumina spinel. The studies revealed that a 99% theoretical density was achieved with 0.5 wt% ZnO after firing at 1550°C. Besides better densification, the samples with ZnO were more resistant to thermal shock than the ZnO free samples. According to the work of Ren et al. [3], lanthanum oxide has also been considered an effective sintering additive. By adding it to magnesia alumina spinel the resulting material had improved density, which is attributed to the formation of $LaAlO_3$ and a defect activation effect. Another oxide studied for its effect on the sintering of $MgAl_2O_4$ was ZrO_2. The work of Mohan and Sarkar [17] showed that ZrO2 in an amount not exceeding 1 wt% enhanced the spinel forming reaction and spinel densification. Nevertheless, with amounts of the additive above this microcracks form, which affects the sintering process.

Despite the breadth of research on the additive-assisted synthesis of $MgAl_2O_4$, limited studies have addressed the influence of ZrO_2, Fe_2O_3, SiO_2, and TiO_2 on the one-step synthesis of $MgAl_2O_4$ from Al_2O_3 and MgO precursors. Consequently, the present study investigates the synthesis of $MgAl_2O_4$ spinel via one-step sintering, producing a baseline sample without additives and four additional samples containing 5 wt% ZrO_2, Fe_2O_3, SiO_2, or TiO_2, respectively. Comprehensive characterization was conducted to determine the phase composition, microstructure, bulk and true densities, as well as open and true porosities of the sintered materials. High-temperature microscopy was employed to identify characteristic thermal events, including high-temperature behavior during synthesis. Additionally, thermodynamic simulations were performed using FactSage 8.3 to predict phase evolution during sintering.

EXPERIMENTAL PART

Sample preparation

In the present study, one type of pressureless sintered high purity stochiometric magnesia alumina spinel [MA] along with four types of modified spinel-based composites [MA_5T, MA_5Z, MA_5F, MA_5S] were synthesized. Aluminum oxide (Chempur, 96% pure Al_2O_3), magnesium oxide (Acros Organics, 98% pure MgO), titanium oxide (Poch, pure p.a.), zirconium oxide (Thermo Scientific, 98.5% pure ZrO_2), iron III oxide (Chempur, 96% pure Fe_2O_3) and silicon dioxide (Poch, pure p.a.) were used as the starting materials. The MA sample was prepared according to the stoichiometric molar ratio of MgO to Al_2O_3 (1:1), as outlined in Table 1. The Al_2O_3 and MgO powders were homogenized using a planetary ball mill for 1 hour at the rotation speed of 300 rpm. The obtained mixture was then then pressed into the form of pellets with a diameter of 20 mm and mass of 3.5 g. These green bodies were then sintered at 1600°C with at the heating rate of 2°C/min and hold time of 10 h. Similarly, the four modified spinel-based composites were prepared by incorporating 5 wt% of the respective modifying oxides – TiO_2, ZrO_2, Fe_2O_3, and SiO_2 – into the MgO-Al_2O_3 mixture for the MA_5T, MA_5Z, MA_5F, and MA_5S samples, respectively, as specified in Table 1. The powders were homogenized by means of a planetary ball mill at 300 rpm for 1 h, then compacted into pellets with a diameter of 20 mm and a mass of 3.5 g, then sintered under the same conditions as the MA sample.

TABLE 1. **Sample designation and composition**

Composition of samples	Designation of samples				
	Pressureless sintered high purity sample	Modified spinel-based composites			
	MA	MA_5T	MA_5Z	MA_5F	MA_5S
	[wt%]	[wt%]	[wt%]	[wt%]	[wt%]
Al_2O_3	72.0	72.0	72.0	72.0	72.0
MgO	28.0	28.0	28.0	28.0	28.0
TiO_2	0.0	5.0	0.0	0.0	0.0
ZrO_2	0.0	0.0	5.0	0.0	0.0
Fe_2O_3	0.0	0.0	0.0	5.0	0.0
SiO_2	0.0	0.0	0.0	0.0	5.0

FactSage 8.3 thermodynamic simulatio

The chemical thermodynamic report containing details of the possible phases during firing versus temperature, element mass fractions and the temperature of the first liquid phase formation were generated by entering the representative oxides of the chemical composition of the samples included in Table 1 into the Equilib module of the FactSage software. Thermodynamic calculations were performed employing the "FactPS", "FTmisc", and "FToxid" databases under the atmospheric pressure of 1 atm. The temperature range investigated spanned from 1000°C to 1700°C, with calculations executed at 100°C intervals. Additionally, changes in the spinel composition at 1600°C were simulated. These options were selected based on multiple preliminary tests, which identified them as providing the most accurate simulation conditions for comparison with experimental data. The relevant results are presented in Section 3.1.

Sample characterization

Both the pressureless sintered high purity stochiometric magnesia alumina spinel [MA] and the modified spinel-based composites [MA_5T, MA_5Z, MA_5F, MA_5S] were analyzed in terms of their phase composition using an X'Pert

Pro PANalytical diffractometer [Cu Kα radiation (λ = 1.54060 Å)] within the range of 2θ values between 5° and 90°. The phase was identified by means of HighScore Plus software. The obtained samples of the final composites after firing at 1600°C were polished under the pressure of 160 N, initially utilizing abrasive disks (grit 120–1200) at 300 rpm with continuous water cooling. Subsequently, the samples were polished with a polishing the cloth and diamond slurry at 150 rpm. The samples were then ultrasonically cleaned in isopropyl alcohol for 30 minutes and coated with carbon. Microstructural and chemical analyses were performed employing a scanning electron microscope (ThermoFisher) and energy dispersive X-ray spectroscopy. The final composites after heat treatment were also characterized in terms of linear dimension change, which was calculated using Eq. 1 and evaluated for open porosity and bulk density by means of the Archimedes method in accordance with the PN-EN 993-1:2019-01 standard. The open porosity and the bulk density were calculated utilizing Eqs. 2 and 3.

$$\Delta L = \frac{(L_1 - L_0)}{L_0} \times 100\% \quad (1)$$

where:
ΔL – percentage change in length [%]
L_0 – original length [mm]
L_1 – length after heat treatment [mm]

$$\rho_b = \frac{m_1}{m_3 - m_2} \times \rho_{liq} \quad (2)$$

$$\pi_a = \frac{m_3 - m_1}{m_3 - m_2} \times 100 \quad (3)$$

where:
m_1 – mass of the dry sample [g]
m_2 – apparent mass of the sample submerged in water [g]
m_3 –mass of the saturated sample [g]
ρ_{liq} – density of the liquid used (water)[g/cm^3]

The true density was measured using helium pycnometry (AccuPyc II 1340, Micromeritics Ltd., UK) with ten purge cycles. Each sample underwent twenty measurement repetitions. The obtained true density values, together with the bulk density results received by means of the Archimedes method, were used to calculate the true porosity of the samples according to Equation 4.

$$\pi_t = \frac{\rho_t - \rho_b}{\rho_t} \cdot 100\% \quad (4)$$

where:
π_t – true porosity [%]
ρ_t – true density [g/cm^3]
ρ_b – bulk density [g/cm^3]

Heating microscopy thermal analysis (HMTA) was conducted to analyze dimensional changes as a function of temperature during heat treatment of the mixture according to Table 1. Mixtures of MgO with Al_2O_3 in a 1:1 ratio, with and without additives, were prepared as dry blends, with the addition of a small amount of dextrin. A small quantity of water was then added to the mixture. Samples were then formed from the resulting mass by pressing. The samples were placed in the furnace chamber, specifically on the corundum pad. The measurement conditions were as follows: from the initial temperature to 100°C at the rate of 4°C/min and from 100°C to the end of the measurement at the rate of 10°C/min. Photographs of the samples were captured utilizing a 720p resolution camera. The relative height changes of the samples (Δh) were calculated according to Eq. 5:

$$\Delta h = \frac{h(T) - h_0}{h_0} \times 100 \quad (5)$$

where:
Δh – change in height
$h(T)$ – height of the sample at the tested temperature
h_0 – height at the initial temperature

RESULTS AND DISCUSSION

FactSage simulations of spinel-based ceramics modified with different components

The presence of phases and the firing behavior of the modified spinel-based ceramics were evaluated using thermodynamic simulation (FactSage 8.3). Calculations in FactSage of the temperature at which the liquid phase as the target phase begins

to form indicated that liquid-phase assisted synthesis occurred in MA_5S, only (Table 2). In the other cases, sintering occurred via the solid-state mechanism as the temperature for the target phase formation exceeded the experimental sintering temperature.

TABLE 2. **Temperature of first liquid phase formation**

Sample				
MA	MA_5T	MA_5Z	MA_5F	MA_5S
Temperature [°C]				
2108	1626	1865	2040	1425

The FactSage calculation results showing the phase fraction as a function of temperature are presented in Figure 1a-e. At the temperature of 1600°C, phases such as Spinel (MA), Ti-Spinel#1 and Pseudobrookite#1 (MA_5T), Spinel and ZrO_2-tetragonal (MA_5Z), Spinel#1 (MA_5F), as well as Spinel and Liquid phase (MA_5S) occurred. A strong correlation was observed between the FactSage calculation results and the XRD analysis, particularly with respect to the main phase of the composites (Table 3). As confirmed by XRD analysis, Ti was incorporated into the spinel structure to form a Ti-bearing spinel (Ti-Spinel#1), while Fe was similarly incorporated, leading to the Fe-bearing spinel (Spinel#1) formation. The FactSage results provided no indication of a solid solution formation between the spinel phase and either ZrO_2 or SiO_2. The results also demonstrate that the trend of the secondary (modifying) phases formation detected by XRD (Figure 2b) is nearly consistent with that calculated by FactSage for the MA_5T composite. The sample with the TiO_2 addition has obvious diffraction peaks of $Mg_{0.6}Al_{0.8}Ti_{1.6}O_5$, which essentially agrees with the results of FactSage predicting the formation of Pseudobrookite#1 with mass fractions of Ti – 0.35524, Al – 0.17005, Mg – 5.1853E-02 and O – 0.42285. According also to Figure 2c, the XRD analysis of the MA_5Z ceramics reveals ZrO_2 both in the monoclinic and tetragonal forms, while the FactSage results indicate the tetragonal form with mass fractions of Zr – 0.73891, Al – 5.8771E-04, Mg – 4.7323E-04 and O – 0.26002. A significant difference was observed between the results of the MA_5S ceramics since quartz in the high and low forms, and forsterite were found by XRD, whereas the liquid phase was calculated by FactSage. Furthermore, the XRD analysis revealed the presence of MgO as an unexpected phase in the MA, MA_5Z, and MA_5F ceramics.

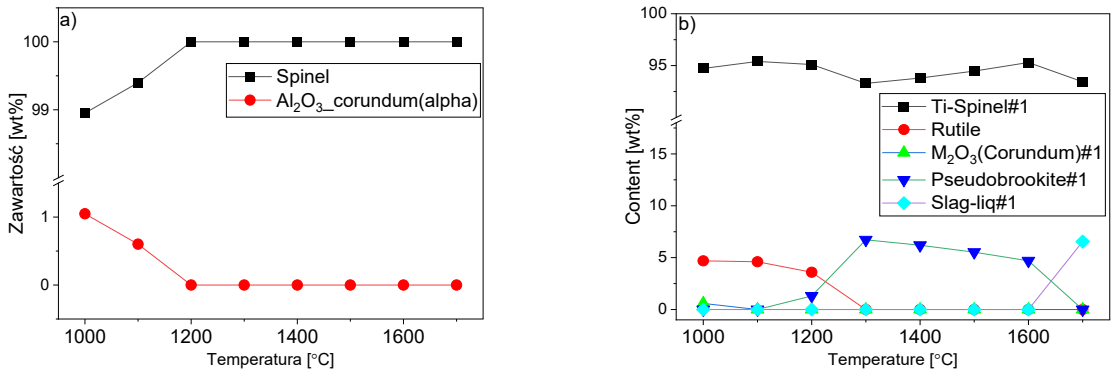

Fig. 1.

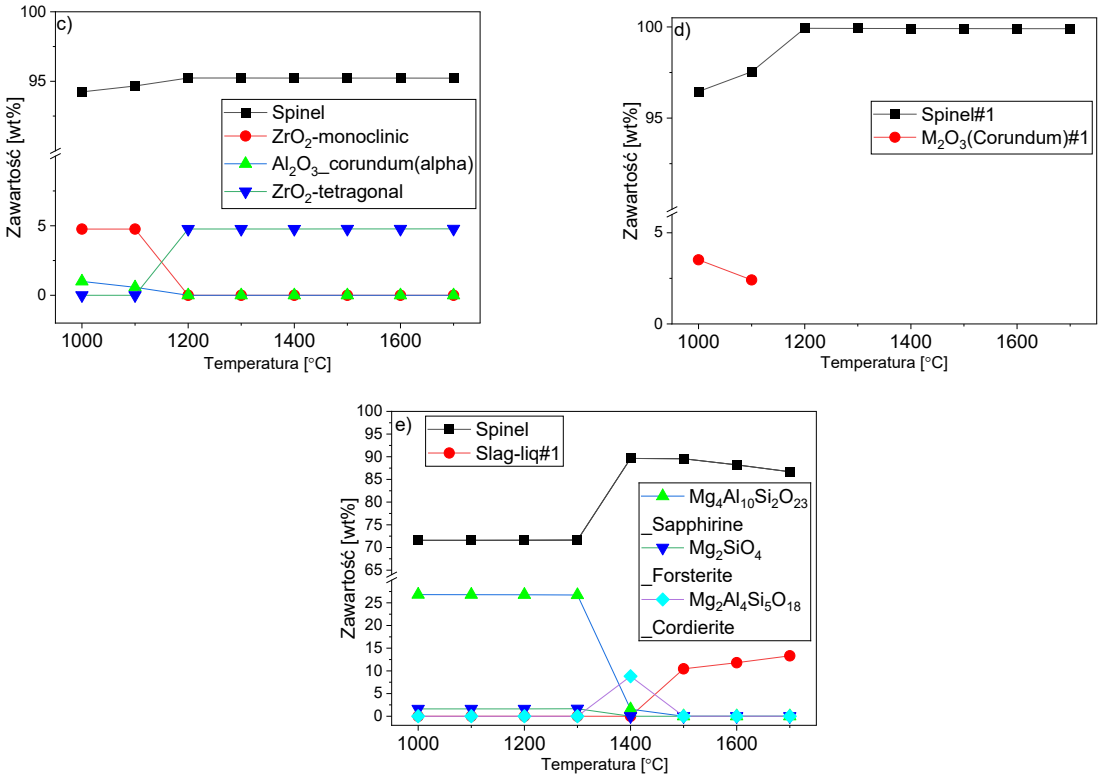

Fig. 1. Phases versus temperature simulated in FactSage for MA (a), MA_5T (b), MA_5Z (c), MA_5F (d) and MA_5S (e) spinel-based ceramics

TABLE 3. **Mass fractions of elements in spinel phase at 1600°C**

System component	Sample				
	MA	MA_5T	MA_5Z	MA_5F	MA_5S
	Mass fraction				
Mg	0.16885	0.16619	0.16884	0.16096	0.16297
Al	0.38106	0.37244	0.38107	0.36326	0.38622
Si	-	-	-	-	-
Fe	-	-	-	3.3338E-02	-
Ti	-	1.2441E-02	-	-	-
O	0.45009	0.44892	0.45009	0.44244	0.45081

Phase composition

XRD analysis of the final composites sintered at 1600°C was carried out to identify the presence of crystalline phases and to evaluate the impact of the modifying ions on the crystal structure of the resulting materials. Figure 2A presents the XRD patterns obtained for all the investigated samples. The diffraction pattern of the MA (Figure 2A-a) sample indicates that the reaction of the starting materials was nearly complete, with only a small amount of unreacted MgO. In the MA_5T (Figure 2A-b) sample, in addition to the characteristic peaks of the $MgAl_2O_4$ phase, we can observe peaks corresponding to a second phase – $Mg_{0.6}Al_{0.8}Ti_{1.6}O_5$ according to the ICDD 00-034-1062 reference card. Furthermore, the main peak related to the spinel phase is shifted towards lower theta angle values, as can be observed in Figure 2B. This shift is likely attributed to the partial dissolving of TiO_2 in the magnesia-alumina spinel.

Ti^{4+} ions can substitute Al^{3+} ions at octahedral sites. Given the larger ionic radius of Ti^{4+} (0.68 nm) compared to Al^{3+} (0.50 nm), this substitution results in an expansion of the unit cell and corresponding changes in the lattice parameters [14]. The XRD phase analysis of the MA_5Z (Figure 2A-c) sample revealed that the diffraction pattern is dominated by reflections corresponding to the $MgAl_2O_4$ spinel phase. Additionally, diffraction lines attributed to monoclinic ZrO_2, $Al_{0.16}Zr_{0.84}O_{1.92}$ and MgO phase were also detected. A slight shift of the main diffraction peak of the spinel phase toward lower 2θ angles can be observed in Figure 2B. According to the ZrO_2–Al_2O_3 phase diagram, the formation of a solid solution of Al^{3+} in the ZrO_2 lattice (Al–ZrO_2(ss)) is possible [19]. Consequently, some Al^{3+} ions originating from the $MgAl_2O_4$ spinel may diffuse into the ZrO_2 phase, which results in a slight shift of the spinel diffraction peak toward lower 2θ angles, indicating a reduced Al content in the spinel structure as can be seen in Figure 2B. In the case of the MA_5F (Figure 2A-d) sample, the diffraction line corresponds to both $MgAl_2O_4$ and a spinel-hercynite solution ($Al_{1.981}Fe_{0.371}Mg_{0.649}O_4$) phase. Additionally, diffraction lines of MgO were identified. and MgO were observed. X-ray diffraction analysis shows that the most intense reflection (100%) for hercynite ($FeAl_2O_4$), according to ICSD card 98-004-0093, is located at 2θ = 36.509°. In the case of the MA sample, the principal diffraction peak appears at 2θ = 36.8156°, which is significantly shifted toward the position characteristic of $MgAl_2O_4$ spinel (2θ = 36.851°, ICSD 00-005-0672). The intermediate peak position indicates that the MA sample constitutes a solid solution between $FeAl_2O_4$ and $MgAl_2O_4$ [20]. A pronounced shift of the main diffraction peak of the spinel phase toward lower 2θ angles was observed, indicating the incorporation of iron ions into the spinel crystal structure [21]. Fe^{3+} and Al^{3+} have similar ionic radii – 0.49 Å for Fe^{3+} [22] and 0.39 Å for Al^{3+} [23]. In the MA_5S (Figure 2A-e) sample, in addition to the primary $MgAl_2O_4$ spinel phase, diffraction peaks corresponding to unreacted SiO_2 and a secondary Mg_2SiO_4 (forsterite) phase were observed. During sintering of the MgO, Al_2O_3, and SiO_2 powders, the predominant reaction occurs between MgO and Al_2O_3, leading to formation of the $MgAl_2O_4$ spinel phase. However, in the MgO–Al_2O_3–SiO_2 system, a concurrent reaction between MgO and SiO_2 also takes place, resulting in the formation of forsterite (Mg_2SiO_4). As reported in some literature sources, this phase can partially dissolve into the spinel structure. At elevated temperatures, an increase in the number of crystallographic defects facilitates mutual solubility between the phases. Crystal defects and dislocations provide the necessary space for the incorporation of foreign species, thus promoting the dissolution process. During this mutual dissolution, silicon ions can incorporate into the spinel structure as dopants, leading to an expansion of the unit cell and, consequently, a shift of the spinel diffraction peaks toward lower 2θ angles [24].

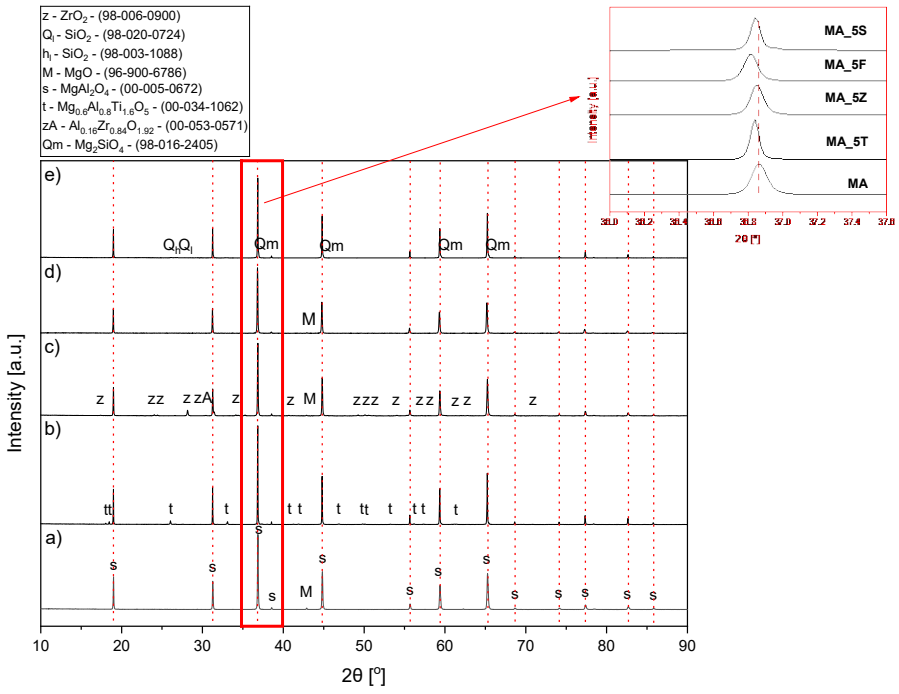

Fig. 2. A) XRD patterns for pressureless sintered high purity stochiometric magnesia alumina spinel and modified spinel-based composites: a) MA, b) MA_5T, c) MA_5Z, d) MA_5F, e) MA_5S, B) comparison of main peak position for all tested samples

SEM-EDS analysis was performed on samples sintered at 1600°C to investigate the influence of the modifying oxide additives on the microstructural evolution and densification behavior of the resulting composite materials. Figure 3a presents an overview of the microstructure of the MA sample, corresponding to pure $MgAl_2O_4$ spinel without the addition of modifying oxides, at 1000× magnification. The sample exhibits a porous microstructure with clearly defined grain boundaries. Porosity is observed not only at the grain boundaries but also within the spinel grains themselves. The microstructure is composed of irregularly shaped grains with sizes ranging from a few micrometers to over 50 µm. At the higher magnification of 5000× (Figure 3b), EDS analysis was conducted, confirming the presence of Mg, Al, and O elements at the analyzed points, indicating that the material consists of mainly $MgAl_2O_4$ spinel. Figure 3 d-g) illustrates the microstructural changes observed for the MA_5T sample containing 5 wt% TiO_2. The microstructure overview at 1000× magnification reveals a porous structure; however, grain boundaries between the spinel grains are not distinctly visible. The pores exhibit irregular shapes and do not exceed 50 µm in size. Additionally, the presence of a secondary phase homogeneously distributed throughout the material is observed. EDS analysis performed at 5000× magnification allowed detailed investigation of the elemental composition of the phases present. The analysis showed that both phases contain Al, Mg, O, and Ti, but differ in their titanium content. The EDS analysis at Point 2 revealed the presence of titanium in microareas of the magnesium aluminate spinel phase, which is consistent with the XRD results showing a shift of the main diffraction peak towards lower 2θ values for the MA_5T sample. The analysis of the secondary phase (Point 1) indicates a significantly higher titanium content, corresponding to the MgO-Al_2O_3-TiO_2

type phase. A comparison of the densification degree reveals that the MA_5T sample exhibits significantly better densification than the pure spinel sample without the modifying additives. This improvement is attributed to the ability of titanium ions to substitute for aluminum ions in the spinel structure, leading to the formation of cation vacancies. Such defects enhance diffusion processes, facilitate mass transport, and thereby promote more effective spinel phase synthesis [14]. Figure 3 h-k presents the microstructure of the MA_5Z sample containing the ZrO_2 additive. The micrograph at 1000× magnification reveals a highly porous structure with clearly defined intergranular boundaries. The microstructure appears homogeneous, with spinel grains uniformly distributed throughout the material and grain sizes not exceeding 50 μm. At this magnification, the presence of a secondary phase, also homogeneously dispersed within the material and located between the grains of the primary phase, can be observed. The micrographs at 5000× magnification, enabled more detailed elemental analysis of the presented phases. EDS analysis performed at Point 2 indicated the presence of Mg, Al and O, and a small amount of zirconium, suggesting that the primary phase corresponds to spinel ($MgAl_2O_4$) with a minor zirconium admixture. EDS analysis at Point 1 corresponding to the modifying phase revealed that this phase is primarily composed of zirconium (Zr) and oxygen (O) and is associated with the presence of magnesium (Mg) and aluminum (Al) from the matrix. Figure 3 l-n presents the microstructure of the MA_5F sample. The micrograph at 1000× magnification reveals that the material exhibits a very high degree of porosity, both at the grain boundaries and within individual grains. The grain sizes range from a few micrometers up to over 50 μm. Overall, the appearance of the microstructure is very similar to that of the MA reference sample. Figure 3m shows the microstructure at 5000× magnification, where EDS analysis performed at Point 1 confirmed the presence of Mg, Al, Fe and O. This can indicate that the primary phase corresponds to magnesium aluminate spinel ($MgAl_2O_4$) with iron ions incorporated into its structure, which was revealed in the XRD analysis. In the case of the MA_5F sample, the modifying additive does not lead to densification of the microstructure of the obtained material. Figure 3 o-s presents micrographs of the microstructure of the MA_5S composite at 1000× magnification. The microstructure of this material differs significantly from that observed for the MA sample. The material exhibits a dense microstructure with only a few pores, ranging in size from several micrometers up to 50 μm. These pores typically possess a regular, oval shape. Notably, grain boundaries are not distinctly visible. The microstructure observed at 5000× magnification reveals that the spinel phase occurs together with the secondary modifying phase. EDS analysis was performed at two points: a at Point 1, corresponding to the secondary phase, confirmed the presence of Si, Mg and O, accompanied by Al, suggesting that this phase is forsterite (Mg_2SiO_4) in the vicinity of $MgAl_2O_4$, consistent with the XRD results. Sodium (Na) ions were also detected, likely originating from starting material contamination. In particular, trace amounts of sodium may be present as impurities in the commercial Al_2O_3 reagent added to the MA_5S composite. Analysis at Point 2 revealed the presence of Mg, Al and O, with a minor amount of Si, indicating the presence of spinel ($MgAl_2O_4$) with potential incorporation of Si into the spinel structure as a dopant, which is consistent with the shift of the spinel diffraction peaks toward lower 2θ values. The observed densification of the microstructure can be attributed to the liquid phase formation in the presence of SiO_2 at grain boundaries during sintering. This liquid phase facilitates the rearrangement and tighter packing of grains, thereby enhancing composite densification [25, 26]. Furthermore, the incorporation of Si^{4+} ions into the spinel structure at high temperatures can promote the mobility of Mg^{2+} and Al^{3+} ions. Enhanced ion mobility supports the formation of a more homogeneous and denser spinel microstructure. The presence of Si^{4+} ions also increases the number of crystal defects, causing lattice distortion that favors ion transport and further densification [27].

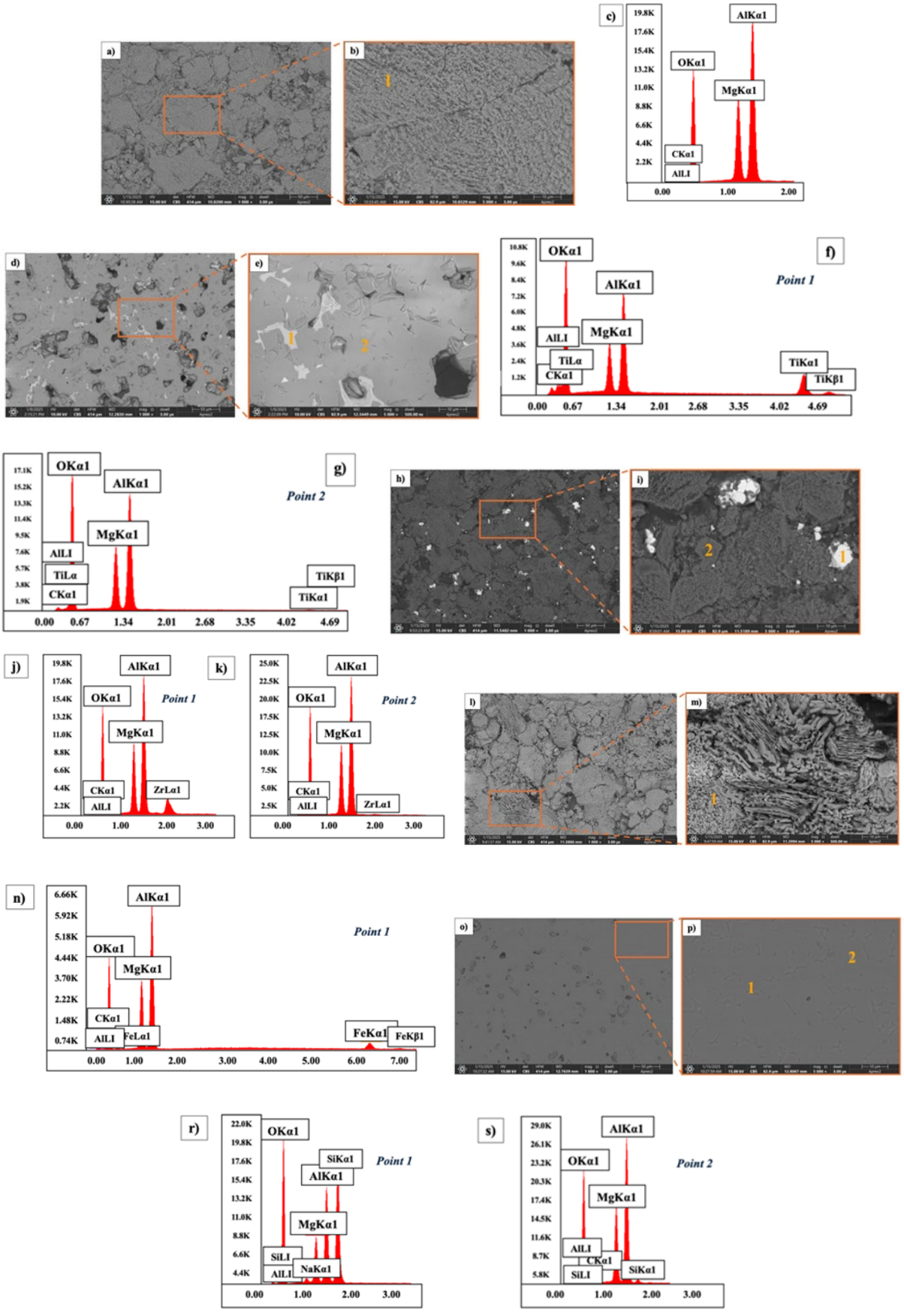

Fig. 3. Figure 3. SEM micrographs and EDS spectraof a-c) MA, d-g) MA_5T, h-k) MA_5Z, l-n) MA_5F, o-s) MA_5S. Dark regions in micrographs correspond to resin-filledpores

TABLE 4. **Elemental composition obtained from EDS analysis at different points on sample surfaces**

EDS spot	O [% wt.]	Mg [% wt.]	Al [% wt.]	Ti [% wt.]	Zr [% wt.]	Fe [% wt.]	Si [% wt.]	Na [% wt.]
MA								
1	43.49	16.98	39.53	-	-	-	-	-
MA_5T								
1	47.63	8.62	17.33	26.42	-	-	-	-
2	48.78	15.60	34.35	1.27	-	-	-	-
MA_5Z								
1	49.03	12.93	28.04	-	10.00	-	-	-
2	50.41	15.17	34.16	-	0.26	-	-	-
MA_5F								
1	49.26	14.50	33.28	-	-	2.96	-	-
MA_5S								
1	50.45	8.47	18.89	-	-	-	21.33	0.86
2	47.65	16.18	35.33	-	-	-	0.84	-

Physical properties

Linear dimension change after firing at 1600°C

The samples were characterized in terms of linear dimensional change after heat treatment at 1600°C. The linear dimensional change was determined as the ratio of the difference between the diameter before and after firing to the initial dimension. Figure 4 presents the dependence of the average linear dimensional change of the composites on the type of additive used. In the case of the MA sample, an expansion of 3.15% after firing was observed. This phenomenon is well known as the reaction between Al_2O_3 and MgO leading to the formation of the $MgAl_2O_4$ spinel is accompanied by volumetric expansion of up to 8% [9, 28]. Additive assisted synthesis can help to mitigate the expansion. The smallest effect on suppressing expansion was observed for the ZrO_2 and Fe_2O_3 additions, with volumetric expansions of 1.28% and 2.33%, respectively, which are nevertheless lower than that of the MA sample. In contrast, in the case of the MA_5S and MA_5T samples, noticeable shrinkage after firing was observed. The linear dimensional changes were -13.35% and -17.70% for MA_5S and MA_5T, respectively. These dimensional changes suggest densification of the samples and improved particle packing.

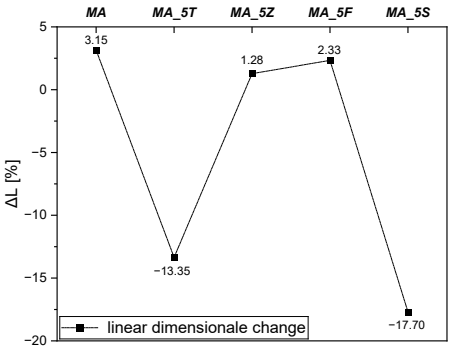

Fig. 4. Comparison of linear dimensional changes after firing at 1600°C for different samples

Density and porosity of pressureless sintered high purity stochiometric magnesia alumina spinel and modified spinel-based composites

Figure 5a,b presents the relationship between the bulk density, true density, as well as both the open and total porosity as a function of the additive used. As shown in Figure 5a, the bulk density of the MA sample was measured at 1.58 g/cm³ (±0.02). Notably, the additions of ZrO_2 and Fe_2O_3 had little impact on increasing the bulk density, with the respective values only slightly higher, reaching 1.66 g/cm³ (±0.0001) and 1.63 g/cm³

(±0.003). In contrast, significant improvement in bulk density was observed with the additions of TiO_2 and SiO_2, resulting in bulk densities of 2.75 g/cm³ (±0.06) and 3.17 g/cm³ (±0.007), respectively. This clearly indicates the strong densification effect induced by these additives. Regarding the true density, the theoretical value of the spinel, calculated based on structural data from the ICSD 98-007-7576 reference card, is 3.58 g/cm³. Interestingly, for the MA, MA_5T, MA_5Z, and MA_5F samples, the measured true densities were slightly higher than the theoretical value, recorded at 3.63 g/cm³, 3.58 g/cm³, 3.69 g/cm³, and 3.65 g/cm³, respectively. However, significant deviation was observed for the MA_5S sample, which exhibited a true density of 3.24 g/cm³. This deviation may be attributed to the presence of an SiO2 -bearing modifying phase, thus reducing the overall true density of the composite material. Moreover, in terms of porosity, illustrated in Figure 5b, the highest total and open porosity was recorded for the MA pure spinel sample, with values of 56.39% (±0.52) and 56.38% (±0.10), respectively. This high porosity is associated with the volumetric expansion that accompanies spinel formation, contributing to increased material porosity. Furthermore, it is noteworthy how the addition of TiO_2 led to a significant reduction in the total and open porosity, down to 23.10% (±1.57) and 21.97% (±1.04), respectively. Even more striking is the effect of SiO_2, which resulted in a drastic reduction in total porosity to 1.97% (±0.21) and open porosity to 1.10% (±0.16). These results clearly confirm that the additions of TiO_2 and especially SiO_2 promote significant microstructural densification, as also evidenced by the SEM micrographs.

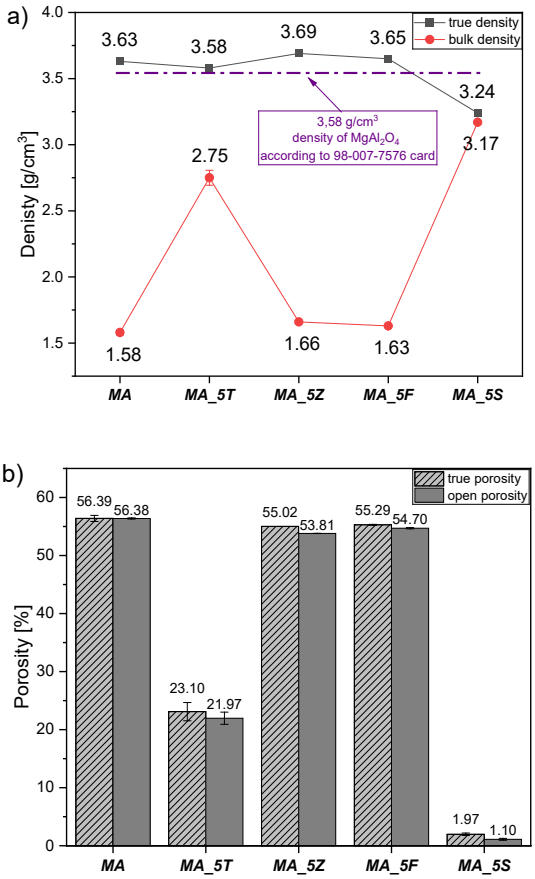

Fig. 5. a) Comparison of bulk and true density values of prepared samples, b) Comparison of open and true porosity values of prepared samples

High-temperature behaviour

HMTA was performed to evaluate dimensional changes of both the pressureless sintered high purity stochiometric magnesia alumina spinel and modified spinel-based composites during their heat treatment process. Table 5 presents the relationship between the temperature and the percentage change in dimensions for each of the investigated samples. Expansion and/or shrinking curves during the heat treatment processes are presented in Figure 6. Positive Δh values indicate volumetric expansion, whereas negative Δh values correspond to shrinkage during thermal processing. Moreover, comparison of heating microscope micrographs obtained at 1450°C for all the samples are shown in Figure 7. For the MA_5S and MA_5T samples, expansion relative to the initial dimensions was observed. In the MA_5S sample, shrinkage initiated at 1305°C (1%) and reached

15% at 1484°C. For MA_5T, shrinkage began at 1355°C (1%), increasing to 2% at 1365°C. In contrast, the MA, MA_5F, and MA_5Z samples exhibited only volumetric expansion. Expansion onset was recorded at 1060°C for MA, and at 950°C for both MA_5F and MA_5Z, with expansion reaching up to 3%. For the reference mixture of magnesium oxide and aluminum oxide without additives, an increase in height was first detected at 1000°C, ultimately reaching 5% at 1430°C. The temperatures corresponding to these dimensional transitions are summarized in Table 4.

Table 5. **Dependence of percentage change in dimensions on temperature for each sample**

Δh [%]	Temperature [°C]				
	MA	MA_5T	MA_5Z	MA_5F	MA_5S
5	1430	-	-	-	-
3	1360	-	950	1060	-
2	1340	-	450	950	-
1	1000	1050	350	650	-
-1	-	1355	-	-	1305
-2	-	1365	-	-	1325
-5	-	-	-	-	1375
-10	-	-	-	-	1435
-15	-	-	-	-	1484

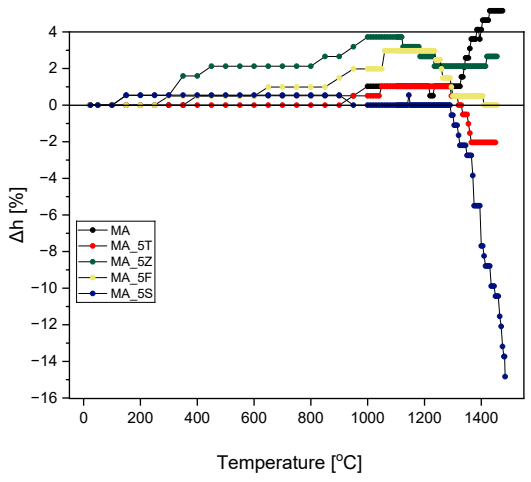

Fig. 6. Shrinkage curves of pressureless sintered high purity stochiometric magnesia alumina spinel and modified spinel-based composites.

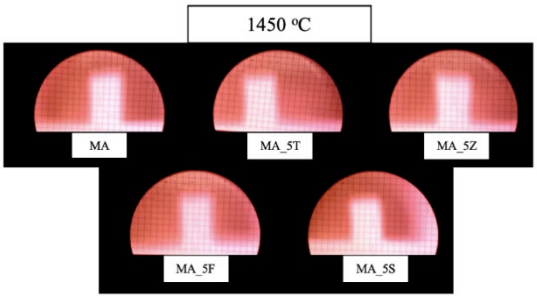

Fig. 7. Heating microscope micrographs of composites samples at 1450°C

CONCLUSIONS

Based on the results of structural analysis (XRD), microstructure studies by the SEM-EDS method, analysis of the physical properties including change in the linear dimensions, density, porosity, high temperature behaviour, and thermochemical simulations performed using FactSage software, the following conclusions were drawn. Modifications to the spinel structure were identified in the presence of iron (Fe^{3+}) and titanium (Ti^{4+}) ions, indicating their partial incorporation into the $MgAl_2O_4$ crystal lattice. This was confirmed by XRD analysis, which revealed a shift of the diffraction pattern toward lower 2θ angles, consistent with the lattice parameter expansion owing to cation substitution. In the MA_5S sample, the shift in the diffraction lines is related to the dissolution process of the Mg_2SiO_4 phase in the $MgAl_2O_4$, while in the sample containing ZrO_2 this shift is due to the extraction of aluminum ions (Al^{3+}) from the spinel structure by zirconium oxide, which was also confirmed by thermochemical calculations in the FactSage software. The highest degree of microstructure densification was observed in the MA_5T and MA_5S samples containing TiO_2 and SiO_2 additives, respectively, suggesting their beneficial effect on the sintering process. It should be noted that only in the case of the MA_5S sample was liquid-phase-assisted sintering involved, whereas for the other samples, densification proceeded by means of solid-state sintering mechanisms. The presence and distribution of secondary (modifying) phases varied depend-

ing on the type of additive introduced into the spinel-based composites. In the samples modified with SiO_2, TiO_2, and ZrO_2, secondary phases were identified primarily along the grain boundaries. Notably, SiO_2 and TiO_2 tended to form intergranular, nearly continuous phases, with SiO_2 showing more pronounced and uniform distribution, which may enhance liquid-phase-assisted sintering. TiO_2, although also present at the grain boundaries, appeared less continuous in comparison. In the case of the Fe-containing samples, no separate secondary phase was detected. Instead, Fe^{3+} ions were incorporated into the spinel lattice, leading to the formation of a solid solution rather than the precipitation of a distinct modifying phase. Dimensional stability after sintering varied significantly among the studied samples. The MA_5Z sample, modified with ZrO_2, exhibited the smallest linear dimensional change, with a modest volume expansion of 1.28%, indicating excellent stability during the sintering process. In contrast, the MA_5S sample, containing SiO_2, showed the greatest linear shrinkage, reaching 17.70%, which can be attributed to the formation of a liquid phase that promotes intensive densification.

Acknowledgements

The research of Dominika Madej was supported by a subsidy from the Polish Ministry of Science and Higher Education. This work was party supported by the program "Excellence Initiative – Research University" for the AGH University of Krakoo (IDUB AGH, grants ID 13447, and ID 12399). The investigations were also supported by the program "Excellence Initiative – Research University" for the AGH University of Krakow, grant ID 12399.

REFERENCES

[1] Ganesh I., A review on magnesium aluminate ($MgAl_2O_4$) spinel: Synthesis, processing and applications. *International Materials Reviews* vol. 58 63–112 (2013).

[2] Tran A.T. *et al.,* Solid-State Reaction Synthesis of $MgAl_2O_4$ Spinel from MgO-Al_2O_3 Composite Particles Prepared via Electrostatic Adsorption. *ACS Omega* 8, 36253–36260 (2023).

[3] Ren X., Ma B., Tian J., Jiang Z., The effects of pre-sintering temperature and La_2O_3 addition on sinterability and corrosion resistance of stoichiometric magnesium aluminate spinel. *Ceram Int* 48, 32470–32478 (2022).

[4] Baruah B., Sarkar R., *Rare-Earth Oxide-Doped Magnesium Aluminate Spinel-an Overview*. Interceram 70, 134–139 (2021).

[5] Sarkar R., *Refractory Applications of Magnesium Aluminate Spinel*. Interceram 64, 136–142 (2015).

[6] Sako E.Y., Braulio M.A.L., Zinngrebe E., Van Der Laan S.R., Pandolfelli V.C., Fundamentals and applications on in situ spinel formation mechanisms in Al_2O_3-MgO refractory castables. *Ceram Int* 38, 2243–2251 (2012).

[7] Han Z., *et al.*, Microstructures and properties of novel lightweight refractory aggregates with microporous MgO@$MgAl_2O_4$ core-shell structures. *J Eur Ceram Soc* 43, 5398–5405 (2023).

[8] Zhihui Z., Li N., *Influence of Mechanical Activation of Al_2O_3 on Synthesis of Magnesium Aluminate Spinel*. *Science of Sintering* vol. 36 (2004).

[9] Tripathi H.S., *et al.*, Synthesis and densification of magnesium aluminate spinel: Effect of MgO reactivity. *Ceram Int* 29, 915–918 (2003).

[10] Mohan S.K., Sarkar R., A comparative study on the effect of different additives on the formation and densification of magnesium aluminate spinel. *Ceram Int* 42, 13932–13943 (2016).

[11] Khomidov F.G., Kadyrova Z.R., Usmanov K.L., Niyazova S.M., Sol-Gel Synthesis of Magnesium Aluminate Spinel as Influenced by Y_2O_3 and Eu_2O_3 Additions. *Inorganic Materials* 59, 627–633 (2023).

[12] Lemeshev D.O., Senina M.O., Pedchenko M.S., Boyko A.V., Transparent ceramic based on magnesium aluminate spinel for armor. in *IOP Conference Series: Materials Science and Engineering*, vol. 525 (Institute of Physics Publishing, 2019).

[13] Canikoglu N., SYNTHESIS OF MAGNESIUM ALUMINATE SPINEL DOPED TiO_2 FROM MAGNESITE WASTE. *Archives of Metallurgy and Materials* 67, 311–316 (2022).

[14] Naghizadeh R., Rezaie H.R., Golestani-Fard F., Effect of TiO_2 on phase evolution and microstructure of $MgAl_2O_4$ spinel in different atmospheres. *Ceram Int* 37, 349–354 (2011).

[15] Ghosh A., Das S.K., Biswas J.R., Tripathi H.S., Banerjee G., *The Effect of ZnO Addition on the Densifcation and Properties of Magnesium Aluminate Spinel*. J. Mater. Sci. Lett. 22, 2011–2014 (2003)

[16] Liu J., Wang Z., Wang X., Liu H., Ma Y., Effects of ZnO addition on the sintering behavior and mechanical properties of magnesium aluminate spinel ceramics. *International Journal of Ceramic Engineering and Science* 1, 51–56 (2019).

[17] Mohan S.K., Sarkar R., Effect of ZrO_2 addition on $MgAl_2O_4$ spinel from commercial grade oxide reactants. *Ceram Int* 42, 10355–10365 (2016).

[18] Baruah B., Yadav N.K., Sarkar R., Effect of Incremental Addition of ZrO_2 on the Densification, Phase Formation, Microstructure, and Strength Development of Pre-reacted Magnesium Aluminate Spinel. *J Mater Eng Perform* (2023) DOI:10.1007/s11665-023-08786-5.

[19] Wu D., *et al.*, Directed laser deposition of Al_2O_3–ZrO_2 melt-grown composite ceramics with multiple composition ratios. *J Mater Sci* 55, 6794–6809 (2020).

[20] Jacob K.T., Patil R., Activities in the spinel solid solution Fe_X $Mg_{1-X}Al_2O_4$. *Metallurgical and Materials Transactions B* 29, 1241–1248 (1998).

[21] Yoon C.M., Choi J.S., Min D.J., Thermodynamic study on the formation of $Mg(Al_{1-x},Fe_x)_2O_4$ between single-crystal $MgAl_2O_4$ and Fe_tO-containing slag at 1550°C. *Ceram Int* 47, 12310–12319 (2021).

[22] Department of Materials – Imperial College London. Atomistic Simulation Group. http://abulafia.mt.ic.ac.uk/shannon/radius.php?Element=Fe. [Accessed 2024]

[23] Department of Materials – Imperial College London. Atomistic Simulation Group. http://abulafia.mt.ic.ac.uk/shannon/radius.php?Element=Al. [Accessed 2024]

[24] Zan W., *et al.*, Synthesis and properties of porous $MgAl_2O_4$-Mg_2SiO_4 refractory aggregates from magnesite tailings and bauxite chamotte. *Ceram Int* (2025) DOI:10.1016/j.ceramint.2025.01.303.

[25] Hu Yan-jun, *et al.*, Enhancing microstructural properties of alumina ceramics via binary sintering aids. *J Cent South Univ* 28, 3705–3713 (2021).

[26] Kim T., Kim D., Kang S., Effect of additives on the sintering of $MgAl_2O_4$. *J Alloys Compd* 587, 594–599 (2014).

[27] Zan W., *et al.*, Preparation and properties of $MgAl_2O_4$ spinel ceramics by double-doped CeO_2 and La_2O_3. *Ceram Int* 49, 15164–15175 (2023).

[28] Saheb N., Alghanim A., Low-temperature and single-step synthesis of fully-dense $MgAl_2O_4$ by reaction spark plasma sintering Al_2O_3 and MgO nano-oxides. *Journal of the Indian Chemical Society* 100, (2023).

